Article

Microgrids Power Quality Enhancement Using Model Predictive Control

Felix Garcia-Torres [1], Sergio Vazquez [2], Isabel M. Moreno-Garcia[3], Aurora Gil [3], Pedro Roncero-Sanchez [4] and Antonio Moreno-Munoz [3]

1 Application Unit, Centro Nacional del Hidrogeno, 13500 Puertollano (Ciudad Real), Spain; felix.garcia@cnh2.es
2 Electronic Department, Universidad de Sevilla, 41092 Sevilla, Spain; sergi@us.es
3 Electronic and Computer Department, Escuela Politécnica Superior, Universidad de Córdoba, Campus de Rabanales, Edificio Leonardo da Vinci, 14071 Córdoba, Spain, amoreno@uco.es
4 Systems Engineering and Automatic Control Department, University of Castilla-La Mancha, Ciudad Real, Spain, pedro.roncero@uclm.es
* Correspondence: felix.garcia@cnh2.es; Tel. +34 926 42 06 82

Abstract: In this paper, the power quality of interconnected microgrids is managed using a Model Predictive Control (MPC) methodology which manipulates the power converters of the microgrids in order to achieve the requirements. The control algorithm is developed for the microgrids working modes: grid-connected, islanded and interconnected. The results and simulations are also applied to the transition between the different working modes. In order to show the potential of the control algorithm a comparison study is carried out with classical Proportional-Integral Pulse Width Modulation (PI-PWM) based controllers. The proposed control algorithm not only improves the transient response in comparison with classical methods but also shows an optimal behavior in all the working modes, minimizing the harmonics content in current and voltage even with the presence of non-balanced and non-harmonic-free three-phase voltage and current systems.

Keywords: Microgrids; Power Quality and Reliability; Model Predictive Control;Interconnected systems; Harmonics; Power System Control

1. Introduction

Power quality and reliability (PQR) will be important factors in the transition towards the smart grid, according to the different national policies the generation should meet the growing demand cleanly, reliably, sustainably and at low cost [1]. In electric power systems, any deviation with respect to the theoretical sinusoidal waveform (produced in the generation centres) is considered to be a perturbation in the power quality of the electrical grid to. The deviation can be given in any of the parameters of the wave: frequency, amplitude, waveform and symmetry between phases. Depending on its grade and the sensitivity of the receptors, this perturbation may have a repercussion on other devices. Adequate quality supply provides the necessary compatibility between all the devices connected to the same grid. In traditional power systems, power quality in a node of the grid is associated with the short circuit power at this point of the grid. Under constant emission higher short circuit power results in better voltage quality. The controllability of fossil-fuel power plants on which the centralized generation and lineal loads are based(with a high resistive component) just cause low level power quality anomalies in comparison with short circuit power in the upstream network [1]. But this scenario has been modified in recent years marking the transition to the smart grid. With independency of the scenario, power quality would be defined by the interaction between the

 doi:10.20944/preprints202101.0003.v1

generation equipment, the consumer devices and the grid. All anomalies should be compensated by the energy storage systems (ESSs). Microgrids can be seen as a key technology to improve PQR aspects of future smart grids. Their ability to work in grid-connected or islanded mode is specially adequate to supply electricity to sensitive loads. In this scenario, enhanced power quality operation of microgrids should be included developing advanced power electronics for interfacing Energy Storage Systems (ESS) which minimize the effects of intermittency of renewable energy systems and compensate the presence of harmonics or unbalanced loads. The controller of these microgrids should include fast transition between grid-connected and islanded mode in order to mitigate the effects of faults in the main grid. Microgrids will also be characterised by a high share of power-electronics devices increasing harmonic levels and possibly causing instability due to interactions among controllers and resonances.

1.1. Literature Review

The microgrids control system must address several aspects with different timescales from their optimization in the day-ahead electrical markets with sample periods of 1 hour towards real-time control of PQR issues with $T_s < 1s$, whose requirements involve different control approaches and different time scales. Fast electrical control of the phase, frequency and voltage of individual resources must be done in time scales lower than second or less, while unit commitment, economic dispatch, demand-side optimization and energy exchanges with the utility grid are performed with longer time scales (minutes or hours). Thus, an extended approach is to develop a hierarchical control structure [2].

In [3], the major issues and challenges in the microgrid control are discussed, and a review of state-of-the-art control strategies and trends is presented; a general overview of the main control principles (e.g., droop control, model predictive control, multi-agent systems) is also included. PQR of microgrids has recently been object of study as can be seen in [4]. PQR aspects of microgrids can be divided in the primary and secondary control levels of microgrids. In the primary control level, the voltage and frequency delivered by the inner loop of each inverter are regulated. Droop control is most commonly used at primary control level. This method assigns to each inverter of the microgrid a droop characteristic based on its generation capabilities [5]. Conventional droop control considers that line impedance is inductive but this assumption is not correct because the output impedance is dependent on the control strategy applied when using power electronics devices. Advanced droop methods are presented in several papers [6], [7]. These methods have the drackback of active and reactive power coupling, which has been addressed by several authors making an approach based on the virtual output impedance method. As a result, the expected voltage can be modified [8]. Secondary control system is usually required to correct the frequency and voltage. Additionally, secondary control algorithms can be used for reactive power compensation [9] and to reduce the harmonics content of the voltage waveform [10]. Most of the existing literature for primary and secondary control in microgrids is based on classical PI-PWM controllers. These kind of controllers do not achieve good results in the transient response which is highly dependent of the tuning of the corresponding parameters of the controllers.

MPC presents several attractive features to be applied in the PQR management of microgrids, appearing as a powerful tool to overcome some of the previously commented problems. The controller can take into account the future behavior of the power inverter despite its complex dynamics. The cost function can integrate multiple criteria, allowing the optimization of important parameters like active and reactive power control, harmonics reduction or ripple minimization. MPC can easily handle the transition between islanded and grid-connected modes achieving faster response than the obtained one by classical PI-PWM controllers. This aspect can be crutial in case of energy supply to critical loads. Its formulation as Finite Control Set (FCS) MPC does not require high computational cost which is a relevant issue concerning control problem of power inverters. The PQR control of the microgrid is established in the secondary and primary control levels. The secondary control level is related with the global control of voltage and frequency in the microgrids including the restoration of voltage/frequency in the transition to islanded mode or the re-synchronization with the main

grid. The primary control directly applies to the power converters of the microgrid [11]. The field of MPC applied to power converters has been applied from two main control strategies: FCS and Continuous Control Set (CCS). FCS is based on the finite number of switching states that a power inverter can adopt. The optimization problem is simplified with the prediction of the converter behavior considering these possible switching states. At each sampling instant, the set of admissible switching sequences is enumerated, the corresponding system response is predicted, the cost function is evaluated and consequently, the sequence which yields the minimal cost is selected [12]. The CCS method sends continuous-time signals as control actions, which are sent to a modulator, and the optimization problem is solved analytically by setting the derivative of the cost function equal to zero in the unconstrained case. Its main advantage is the use of longer control horizons since an analytical solution is provided. Nevertheless, with complex topologies of power inverters this methodology presents difficulties to create an appropriate model of the plant, being also necessary higher computation resources. A basic application for this kind of controllers can be found in [13]. The last studies related to power quality enhancement with power inverters search the harmonic compensation using four-leg voltage source inverter topologies with active neutral control. In [14] an active power filter implemented with a four-leg voltage-source inverter (VSI) using an MPC scheme is presented for grid-connected applications. The paper presented [15] applies similar methodology in the new implementation of the finite control states set model predictive control (FS-MPC) applied to three-level four-leg flying capacitor converter (FCC) operating as a shunt active power filter. The obtained results by the control algorithm improves the current tracking capability, and transient response. Nevertheless, the use of FCS-MPC controller achieve bad results in the THD content. In [16], a cascade-free fuzzy FCS-MPC is proposed for neutral point-clamped power inverters with low switching frequency (SF). The main objective of the proposed method is to achieve a low SF operation. The cost function is formulated to reduce the SF, and a fuzzy logic control (FLC) technique is employed to choose the weighting factors dynamically. The article presented in [17] proposes a novel flexible reference current generation technique by using a tuning parameter to reduce the active power oscillation flexibly. The generated reference current comprises not only the positive and negative sequence currents but also lower order harmonic components. A flexible multifrequency reference current computation technique for the unbalanced and distorted grid conditions is developed using MPC control techniques. The experimental and simulation results successfully validated the trade off between the low frequency power oscillations and current THD which was established using a tuning parameter. Therefore, with the proposed scheme active power oscillations can be reduced in microgrids scenarios. In [18], a composite selective harmonic elimination pulse-width modulation (SHE-PWM) and model predictive control (MPC) for seven-level hybrid-clamped (7L-HC) inverters is presented. The proposed methodology achieves as results a low switching frequency with good harmonic performance with a reduced computational burden. In [19], a strategy that combines FCS-MPC with SHE modulation pattern in its formulation is proposed to govern multilevel power converters. The proposed methodology is based on considering a desired operating point for the system state (converter current reference), an associated predefined SHE voltage pattern is obtained as a required steady-state control input reference. Then, the cost function is formulated with the inclusion of both system state and control input references. The obtained experimental results present fast dynamic response while a predefined voltage and current spectrum with low switching frequency is achieved in steady-state. In [20], a model predictive power control (MPPC) scheme and a model predictive voltage control (MPVC) scheme is presented. The proposed methodology consists on ontrolling the bidirectional buck-boost converters of the battery energy storage systems based on the MPPC algorithm, the fluctuating output from the renewable energy sources can be smoothed, while stable dc-bus voltages can be maintained as the inverters inputs. Then, the parallel inverters are controlled by using a combination of the MPVC scheme and the droop methodto ensurestable ac voltage output and proper power sharing.Compared with the traditional cascade control,the proposedmethodissimpler and

 doi:10.20944/preprints202101.0003.v1

shows better performance, which isvalidated insimulation on MATLAB/Simulink and on Real-Time Laboratory (RT-LAB) platform.

Microgrids consist of multiple parallel-connected distributed generators, storage devices, or controllable loads which are able to operate in both grid-connected and islanded modes, in a coordinate mode. In islanded mode, it is required to maintain system stability and power quality among the multiple parallel interconnected devices. Deficit balances in the active and reactive power between the different components of the microgrids, due to several aspects such as the influence of impedance mismatch of the feeders and the different ratings of the distributed units can lead to poor power quality indexes which can damage the connected devices to same microgrid AC/DC bus. In connected mode, unbalances in the active/reactive power can affect to the schedule carried out with the main grid in the tertiary control. The increasing presence of non-linear loads and umbalance loads could further affect to the global power balance in the microgrid. For these reasons, secondary control levels have been proposed based on different methodologies such as enhanced droop-control, network-based control methods, improved hierarchical control approaches based on graph theory, multi-agent system, gain scheduling methods, etc. In the existing literature, several authors propose MPC-based controllers applied to voltage and frequency regulation problems in microgrids can be found. In [21] an MPC-based controller and a Smith predictor (SP) based controller are applied to the secondary level of the microgrid. The results of this work prove that with the proposed methodology, nominal values of frequency can be reached with a faster speed but fewer oscillations during load variations. In addition, the MPC-controller with the SP solves the problems brought by communication delays. In [22], a secondary control level is proposed linked to the schedule carried out in the tertiary control level of the microgrid. The microgrid includes hybrid ESS and the different operation issues of each one of the ESS technologies is included to carry out the real-time power balance of the microgrid. In [23], a fuzzy adaptive model predictive approach for load frequency control of an isolated microgrid is proposed. The frequency deviation problem is solved using a centralized MPC which is made adaptable by dynamically adjusting its parameters using a fuzzy controller. In [24], a distributed secondary control scheme for both voltage and frequency control in autonomous microgrids. The algorithm incorporates predictive mechanisms into distributed generations, the secondary voltage control is converted to a tracker consensus problem of distributed model predictive control, with the synchronous convergence procedure for voltage magnitudes to the reference value drastically accelerated at a low communication cost. In [25], a virtual inertia control-based MPC for microgrid frequency stabilization a system for microgrids is developed. The proposed MPC-based virtual inertia control is tested for several mismatched parameters of the microgrid, wind power, and load disturbances. The proposed MPC-based virtual inertia control is able to reduce and stabilize frequency deviation of the microgrid and gives robustness to the system subjected to uncertainties and disturbances over the fuzzy logic and conventional virtual inertia systems, enhancing the stability and resiliency of the microgrid. In [26], a DMPC-based strategy for regulating the frequency and average voltage and achieving real and reactive power consensus in the microgrid is presented. The proposed methodology is based on droop, power transfer and phase angle equations used to solve the DMPC. The formulation includes explicit operational constraints to ensure the operation of the microgrid within feasible ranges. The controller is also able to modify its adjacency matrix in response to either electrical or communications disturbances. The performed simulations and experimental tests show that the use of the proposed controller allows achieving the regulation and consensus objectives satisfying the operational constraints. The presented results improve the microgrid behavior against electrical disturbances, such as load changes or disconnecting/reconnecting of distributed generators and communication issues such as latency and data packet losses.

1.2. Main Contributions

In AC microgrids, the final power quality obtained in the microgrid depends on the exchanged power flow between its local devices connected and the grid. An appropriate energy storage system

Preprints (www.preprints.org) | NOT PEER-REVIEWED | Posted: 4 January 2021 doi:10.20944/preprints202101.0003.v1

(ESS) connected to a voltage source inverter (VSI) can be used to enhance the power quality of the microgrid. The final result not only depends on the topology of the VSI but also on its control system. With the aim to obtain an optimal power flow in the microgrid, a four wire VSI with active neutral control is selected in order to integrate unbalanced and non-linear loads. The VSI response is improved using an innovative MPC controller to manage the power quality of the microgrids and their power exchange with the main grid or with the neighbor microgrids. The studied references in previous section do not solve completely the problem of transient response due to the fact that droop controls and/or PI-based controller are applied. The state of the art of the MPC controllers applied to primary control of the microgrid use the instantaneous expressions for active and reactive power expressed with Park/Clark's transformation. These expressions can only be computed for balanced and harmonic-free three-phase voltages. Based on the MPC strategy which uses Fourier's transform presented in [27], this paper develops a primary MPC using the expression for active and reactive powers of the voltage-current pairs calculated at fundamental frequency. The presented method for the voltage control of the microgrid in [27] is extended here to include non-linear and non-balanced loads developing an MPC-controller applied to four-wire three-phase voltage source inverter with active control of the neutral point. The method is also expanded to include the islanded and grid-connected operation modes. Different case studies to demonstrate the enhanced power quality operation of the microgrid such as harmonic mitigation, unbalanced and non-linear loads in both modes are shown. The behavior of the control algorithm to achieve a fast transition from grid-connected to islanded mode and vice versa is presented. The method is also expanded to be used in the case of interconnected microgrids working under a blackout of the main grid.

The paper is organized as follows: Section II provides a description of the controller design, while Section III presents the results for the different case studies. Finally, Section IV outlines the conclusions.

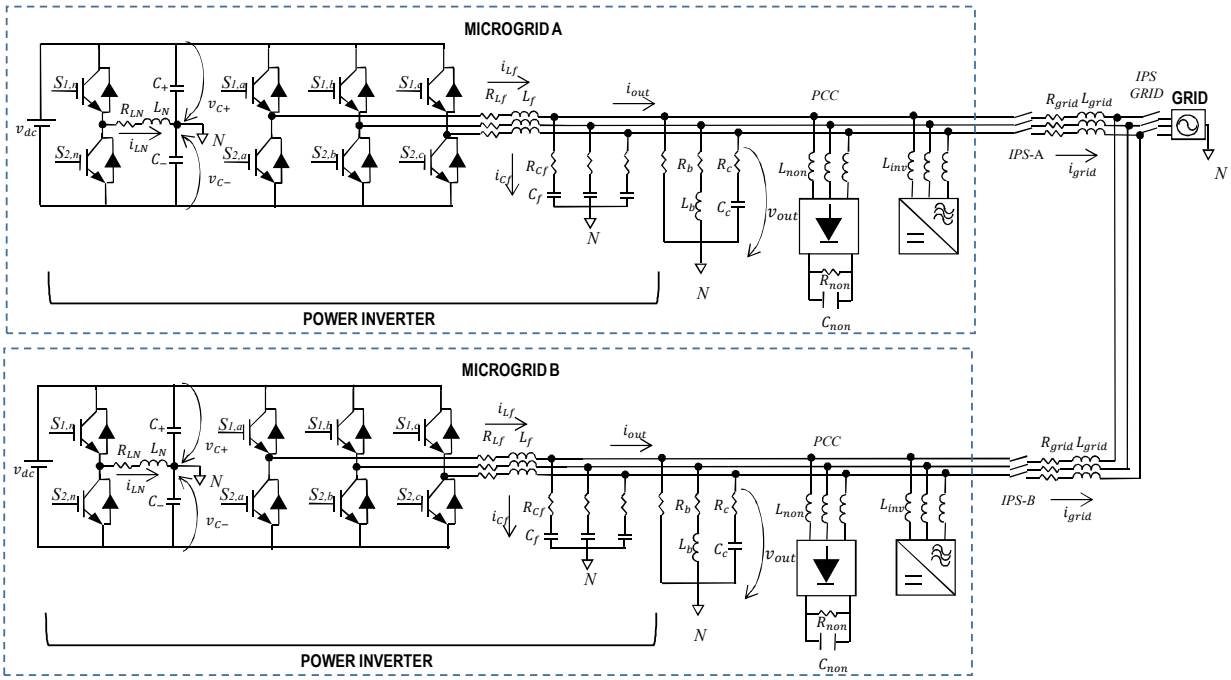

Figure 1. Inteconnected microgrids object of study

Preprints (www.preprints.org) | NOT PEER-REVIEWED | Posted: 4 January 2021 doi:10.20944/preprints202101.0003.v1

2. Controller Design

The topology of the interconnected microgrids object of this paper is shown in Fig. 1. As can be seen in Fig. 1, there are three intelligent power switches (IPS) installed to isolate or connect the working mode of each microgrid with the main grid and/or with the neighbor microgrid. In AC microgrids, the final power quality obtained in the microgrid depends on the exchanged power flow between its local devices connected and the grid. An appropriate energy storage system (ESS) connected to a voltage source inverter (VSI) can be used to enhance the power quality of the microgrid. The final result not only depends on the topology of the VSI but also on its control system. With the aim to obtain an optimal power flow in the microgrid, a four wire VSI with active neutral control is selected in order to integrate unbalanced and non-linear loads. The VSI response is improved using an innovative MPC controller to manage the power quality of the microgrids and their power exchange with the main grid or with the neighbor microgrids. The block diagram of the controller is exposed in Fig. 2.

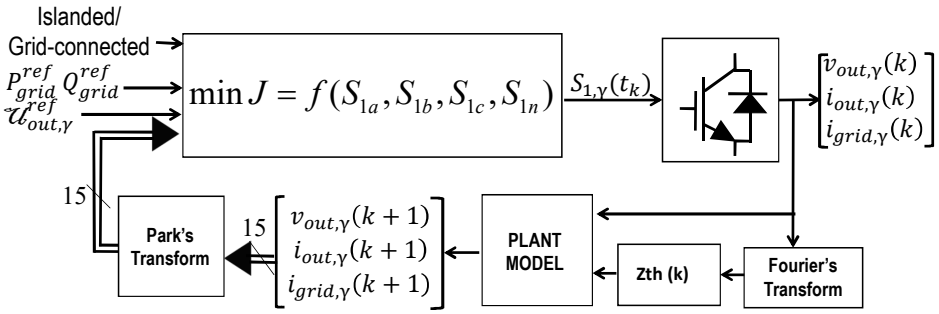

Figure 2. Block Diagram

The first step of the controller is to calculate the Fourier analysis of the current and voltage output at the current sample instant k. With these measurements the Thevenin-equivalent impedance is calculated at the output of the inverter. With this equivalent impedance the output current and voltage prediction is carried out which is included in the cost function to be minimized. Finally the optimal gate-signal combination is calculated in the MPC controller.

2.1. Fourier Expressions

As explained in the previous section, the instantaneous active power and reactive power expressed with Park's transformation can only be computed for balanced and harmonic-free three-phase voltages. While it is still necessary to compute the active and reactive powers associated with a periodic set of three-phase voltages and currents equations. This is done through the Fourier analysis of the current and voltage signals per phase. As is well-known, a signal $y(t)$ can be expressed by a Fourier series of the form:

$$y(t) = \frac{a_0}{2} + \sum_{n=0}^{\infty} a_n \cos(n\omega t) + b_n \sin(n\omega t) \tag{1}$$

where n represents the rank of the harmonics (n = 1 corresponds to the fundamental component). The magnitude and phase of the selected harmonic component can be calculated by the next equations:

$$|\mathscr{Y}_n| = \sqrt{a_n^2 + b_n^2}; \; \angle\mathscr{Y}_n = \arctan\left(\frac{b_n}{a_n}\right) \tag{2}$$

where $\mathscr{Y}_n$ is the Fourier's expression of the signal y(t), which can be expressed in cartesian coordinates with the following expressions:

$$\mathrm{Im}(\mathscr{Y}_n(t)) = a_n^y = \frac{2}{T}\int_{t-T}^{t} y(t)\cos(n\omega t)dt; \tag{3}$$

Preprints (www.preprints.org) | NOT PEER-REVIEWED | Posted: 4 January 2021 doi:10.20944/preprints202101.0003.v1

$$\mathrm{Re}(\mathscr{Y}_n(t)) = b_n^y = \frac{2}{T}\int_{t-T}^{t} y(t)\sin(n\omega t)dt \tag{4}$$

being $T = 1/f$ the corresponding period to the fundamental frequency. The upper index y is related to the signal $y(t)$ in which the Fourier analysis is developed. Using expressions (2), for the voltage and current signals, the value of this signal expressed in the Fourier's domain $\mathscr{U}(t)$ and $\mathscr{I}(t)$ can be obtained. The equivalent Thevenin's impedance calculated for the fundamental frequency can be estimated in polar coordinates:

$$\left|Z_n^{th}(t)\right| = \frac{\sqrt{(a_n^v(t))^2 + (b_n^v(t))^2}}{\sqrt{(a_n^i(t))^2 + (b_n^i(t))^2}} \tag{5}$$

$$\varphi_n^{th}(t) = \angle Z_n^{th}(t) = \arctan\left(\frac{b_n^v(t)}{a_n^v(t)}\right) - \arctan\left(\frac{b_n^i(t)}{a_n^i(t)}\right) \tag{6}$$

The upper index v and i are related to the output voltage and output current of the inverter. Expressing $Z_{th,n}(k)$ in cartesian coordinates the equivalent resistance and the equivalent impedance can be obtained:

$$Z_n^{th}(t) = R_n^{th}(t) + jX_n^{th}(t) \tag{7}$$

Particularizing for $n = 1$, depending of the value of $X^{th}(t)$ an equivalent inductance or capacitance can be obtained, in these cases when $\mathrm{sign}(X^{th}(t)) = \mathrm{sign}(R^{th}(t))$ expression (8) and using the relationship given in (9) when $\mathrm{sign}(X^{th}(t)) \neq \mathrm{sign}(R^{th}(t))$:

$$L^{th}(t) = \frac{X^{th}(t)}{2\pi f};\ C^{th}(t) = 0 \tag{8}$$

$$L^{th}(t) = 0;\ C^{th}(t) = -X^{th}(t)\cdot 2\pi f \tag{9}$$

The expression for active and reactive powers of the voltage-current pairs calculated at fundamental frequency can be computed (being $\varphi_{j,n}^{th}(t_{k+1})$ the phase of Thevenin's impedance evaluated at $n = 1$):

$$P(t) = \frac{|\mathscr{U}(t)||\mathscr{I}(t)|}{2}\cos(\varphi_1^{th}(t)) \tag{10}$$

$$Q(t) = \frac{|\mathscr{U}(t)||\mathscr{I}(t)|}{2}\sin(\varphi_1^{th}(t)) \tag{11}$$

Expressions (10) and (11) are valid for all the cases, including non-balanced and non-harmonic-free three-phase voltages and currents systems.

2.2. Predictive Model of the VSI

The model of the plant can be obtained as a function of its decision variables (gate signals of each leg S_{1a}, S_{1b}, S_{1c} and S_{1n}), the set of state variables composed by the inductor currents or capacitor voltages and the output currents and voltages of the inverter per phase [v_{C+}, v_{C-}, i_{LN}, v_{Cf}, i_{Lf}, $i_{out,j}$, $v_{out,j}$], following the expressions (12)-(17). (Notice that $\Delta y(k+1) = y(k+1) - y(t_k)$)

$$v_{dc}(k+1) = +v_{C+,N}(k+1) - v_{C-,N}(k+1) \tag{12}$$

$$i_{Cj}(k+1) = C_j\frac{v_{Cj,N}(k+1) - v_{Cj,N}(t_k)}{T_s}|_{j=+,-} \tag{13}$$

$$\begin{aligned} &v_{C+,N}(k+1)\cdot S_{1n}(k+1) + v_{C-,N}(k+1)\cdot(1 - S_{1n}(k+1)) \\ &= R_{L_N}\cdot i_{L_N}(k+1) + L_N\frac{\Delta i_{L_N}(k+1)}{T_s} \end{aligned} \tag{14}$$

Preprints (www.preprints.org) | NOT PEER-REVIEWED | Posted: 4 January 2021 doi:10.20944/preprints202101.0003.v1

$$i_{C-}(k+1) + i_{C+}(k+1) + i_{L_N}(k+1) = -\sum_{j=a,b,c} i_{out,j}(k+1) - \sum_{j=a,b,c} i_{C_f,j}(k+1) \tag{15}$$

The values of the inductor currents of the LC-filter ($i_{L_{fj}}(k+1)$) can be predicted with the following equations:

$$\begin{aligned} v_{out,jN}(k+1) &= v_{C+}(k+1)\cdot S_{1j}(k+1) \\ &+ v_{C-}(k+1)\cdot(1-S_{1j}(k+1)) - L_f\frac{\Delta i_{L_{fj}}(k+1)}{T_s} \\ &- R_{L_f}\cdot i_{L_{fj}}(k+1)|_{j=a,b,c} \end{aligned} \tag{16}$$

$$i_{C_{fj}}(k+1) = C_f\frac{\Delta v_{out,j}(k+1) - R_{C_f}\Delta i_{C_{fj}}(k+1)}{T_s} \tag{17}$$

$$i_{grid,j}(k+1) + i_{\mu grid,j}(k+1) = i_{L_f,j}(k+1) - i_{C_f,j}(k+1) \tag{18}$$

Under the assumption $Z_n^{th}(k+1)$=$Z_n^{th}(t_k)$ and approaching the equivalent Thevenin's impedance only for the fundamental frequency, the relationship (19) can be obtained in case that $X_j^{th}(k) \geq 0$ and (20) when $X_j^{th}(k) < 0$:

$$\begin{aligned} v_{PCC,j}(k+1) &= R_j^{th,\mu grid}(k)\cdot i_{\mu grid,j}(k+1) \\ &+ L_j^{th,\mu grid}(k)\frac{i_{\mu grid,j}(k+1) - i_{\mu grid,j}(k)}{T_s}\Bigg|_{j=a,b,c} \end{aligned} \tag{19}$$

$$\begin{aligned} &i_{\mu grid,j}(k+1)\Big|_{j=a,b,c} = \\ &C_j^{th,\mu grid}(k)\frac{\Delta[v_{PCC,j}(k+1) - R_j^{th,\mu grid}(k)\cdot i_{\mu grid,j}(k+1)]}{T_s} \end{aligned} \tag{20}$$

In those cases, when the inverter works tied to the main grid:

$$\begin{aligned} v_{grid,j}(k+1) - v_{PCC,j}(k+1) &= R^{grid}\cdot i_{grid,j}(k+1) \\ &+ L_j^{grid}\frac{i_{grid,j}(k+1) - i_{grid,j}(k)}{T_s}\Bigg|_{j=a,b,c} \end{aligned} \tag{21}$$

2.3. Cost Function for the Islanded Mode

In this working mode the inverter object of this study has to manage the voltage waveform in which concerns to magnitude, frequency, harmonics content and phase equilibrium. In order to achieve these criteria, the cost function expressed in (22) is divided into three main parts: J_{isl}^{wave} which manages the waveform of the output voltage, J_{isl}^{harm} which minimizes the harmonics content and J_{isl}^{bal} which controls the balance between phases. In order to use the predictive model of the inverter, the assumption that between two sample instants $Z_{out,\alpha}^{th}(k+1) = Z_{out,\alpha}^{th}(k)$ has to be used in the predictive model of the inverter.

$$\min_{\mathbf{s}(k)} J_{isl}(k) = \min_{\mathbf{s}(k)} \left(J_{isl}^{wave}(k) + J_{isl}^{harm}(k) + J_{isl}^{bal}(k) \right) \tag{22}$$

Preprints (www.preprints.org) | NOT PEER-REVIEWED | Posted: 4 January 2021 doi:10.20944/preprints202101.0003.v1

$$
\begin{aligned}
J_{isl}^{wave}(k) = \sum_{\alpha=a,b,c} \Big[& w_{isl}^{inst} \left(v_{out,\alpha}(k+1) - v_{out,\alpha}^{ref}(k+1) \right)^2 \\
& + w_{isl,\alpha}^{cycle} \left(\Re e(\mathscr{U}_{out,\alpha}(k+1)) - \Re e(\mathscr{U}_{out,\alpha}^{ref}(k+1)) \right)^2 \\
& + w_{isl,\alpha}^{cycle} \left(\Im m(\mathscr{U}_{out,\alpha}(k+1)) - \Im m(\mathscr{U}_{out,\alpha}^{ref}(k+1)) \right)^2 \Big]
\end{aligned} \tag{23}
$$

At each sample instant, the voltage reference is calculated and imposed in the first term of (23) minimizing the difference between the predicted voltage and the calculated reference. In order to minimize the steady-state error the second term of (23) is added, correcting this error with the complete fundamental cycle computation.

$$
\begin{aligned}
J_{isl}^{harm}(k) = \sum_{\alpha=a,b,c} \Big[& w_{isl,\alpha}^{v} \left(\Delta v_{out,\alpha}(k+1) \right)^2 \\
& + w_{isl,\alpha}^{i} \left(\Delta i_{out,\alpha}(k+1) \right)^2 \Big] \\
& + w_{isl}^{cap} \left(v_{C+}(k+1) - v_{C-}(k+1) \right)^2
\end{aligned} \tag{24}
$$

The first and second term of (24) minimize the voltage and current abrupt variations between two sample instants avoiding the harmonics content in both voltage and current. The third term manages the balance of voltage for the neutral point.

$$
J_{isl}^{bal}(k) = \sum_{\alpha=a,b,c}^{\beta=b,c,a} w_{isl}^{bal} \left(|\mathscr{U}_{out,\alpha}(k+1))| - |\mathscr{U}_{out,\beta}(k+1)| \right)^2 \tag{25}
$$

When unbalanced loads are connected to the inverter the voltage magnitude between phases is decompensated. In order to control these situations the term expressed in (25) is included in the cost function.

2.4. Cost Function for the Grid-Connected Mode

In grid connected mode, it is assumed that due to the fact that the voltage reference is imposed by the main grid. Under the assumption of robustness in the voltage waveform provided by the main grid and considering that Park?s transformation is a rotational reference frame, it is considered that between two sample instants the *dqo*-voltage is constant. Under this assumption and using the predictive model can be obtained the output currents $i_{out,\gamma}(k+1)$ $i_{grid,\gamma}(k+1)$ of each phase.

The controller receives the set-point for the exchange of active and reactive powers with the main grid $(P_{grid,\alpha}^{ref}(k+1), Q_{grid,\alpha}^{ref}(k+1))$. Due to the fact that $\mathscr{U}_{grid,\alpha}^{ref}(k)$ is imposed by the main grid and supposed constant between two sample instant , it can easily obtained the reference current $\mathscr{I}_{grid,\alpha}^{ref}(k)$ with the following equations:

$$
P_{grid,\alpha}^{ref}(k) = \frac{|\mathscr{U}_{grid,\alpha}^{ref}(k)||\mathscr{I}_{grid,\alpha}^{ref}(k)|}{2} \cos(\varphi_{grid,\alpha}^{ref}(k)) \tag{26}
$$

$$
Q_{grid,\alpha}^{ref}(k) = \frac{|\mathscr{U}_{grid,\alpha}^{ref}(k)||\mathscr{I}_{grid,\alpha}^{ref}(k)|}{2} \sin(\varphi_{grid,\alpha}^{ref}(k)) \tag{27}
$$

The current references are calculated as follows:

$$
\begin{aligned}
& i_{grid,\alpha}^{ref}(k+1) = \\
& |\mathscr{I}_{grid,\alpha}^{ref}(k+1)| \sin(\omega(k+1+D_\alpha) + \varphi_{grid,\alpha}^{ref}(k+1))
\end{aligned} \tag{28}
$$

Preprints (www.preprints.org) | NOT PEER-REVIEWED | Posted: 4 January 2021 doi:10.20944/preprints202101.0003.v1

A digital delay D_α has to be included which is adaptive with $Z^{th}_{out,\alpha}(k)$. As done for the case of islanded mode, the cost function in grid-connected mode is divided into three parts:

$$\min_{\mathbf{s}(k)} J_{conn}(k) = \min_{\mathbf{s}(k)} \left(J^{wave}_{conn}(k) + J^{harm}_{conn}(k) + J^{bal}_{conn}(k) \right) \tag{29}$$

$$\begin{aligned} J^{wave}_{conn}(k) = \sum_{\alpha=a,b,c} \Big[& w^{inst}_{conn} \left(i_{grid,\alpha}(k+1) - i^{ref}_{grid,\alpha}(k+1) \right)^2 \\ & + w^{cycle}_{conn,\alpha} \left(\Re e(\mathscr{I}_{grid,\alpha}(k+1)) - \Re e(\mathscr{I}^{ref}_{grid,\alpha}(k+1)) \right)^2 \\ & + w^{cycle}_{conn,\alpha} \left(\Im m(\mathscr{I}_{grid,\alpha}(k+1)) - \Im m(\mathscr{I}^{ref}_{grid,\alpha}(k+1)) \right)^2 \Big] \end{aligned} \tag{30}$$

The procedure to formulate (30) is similar to the one carried out for (23). At each sample instant, the current reference is calculated and imposed in the first term of (30), minimizing the difference between the predicted current exchange with the main grid and the reference calculated. In order to minimize the steady state error the second term of (30) is added correcting this error with the complete fundamental cycle calculus done for the current exchange with the main grid expressed in Fourier's domain.

$$\begin{aligned} J^{harm}_{conn}(k) = \sum_{\alpha=a,b,c} \Big[& w^{v}_{conn,\alpha} \left(\Delta v_{out,\alpha}(k+1) \right)^2 \\ & + w^{i}_{conn,\alpha} \left(\Delta i_{grid,\alpha}(k+1) \right)^2 \Big] \\ & + w^{cap}_{isl} \left(v_{C+}(t_{k+1}) - v_{C-}(t_{k+1}) \right)^2 \end{aligned} \tag{31}$$

The second part of the cost function in grid-connected mode (31) minimizes the harmonic injection in current to the grid, as well as the voltage variations in the microgrid. It also balances the neutral point of the inverter. Finally, when unbalanced loads are connected to the microgrid they can affect to balance in the active and reactive power injected to main grid. For this purpose the term of the cost function expressed in (32) is included.

$$\begin{aligned} & J^{bal}_{conn}(k) = \\ & \sum_{\alpha=a,b,c}^{\beta=b,c,a} w^{bal}_{conn} (P_{grid,\alpha}(k+1)) - P_{grid,\beta}(k+1)))^2 \\ & + \sum_{\alpha=a,b,c}^{\beta=b,c,a} w^{bal}_{conn} (Q_{grid,\alpha}(k+1)) - Q_{grid,\beta}(k+1)))^2 \end{aligned} \tag{32}$$

2.5. Cost Function for the Interconnected Mode

The interconnected mode can be considered as a hybrid mode between the connected and the islanded mode since there does not exist a main grid who imposes the references in voltage and frequency but there can be energy exchange between the interconnected microgrids. Due to the fact that there is not a main grid both microgrids have to work controlling the voltage and the frequency, the so-called multi-master mode.

$$\begin{aligned} \min_{\mathbf{s}(k)} J^{(X)}_{inter}(k) = \min_{\mathbf{s}(k)} \Big(& J^{(X),wave}_{isl}(k) + J^{(X),harm}_{isl}(k) \\ & + J^{(X),bal}_{isl}(k) + \sum_{\gamma=a,b,c} (i^{(X)->(Y)}_{\gamma}(k))^2 \Big) \end{aligned} \tag{33}$$

Preprints (www.preprints.org) | NOT PEER-REVIEWED | Posted: 4 January 2021 doi:10.20944/preprints202101.0003.v1

The notation (X) refers to the microgrids (A) and (B) and the terminology $(X)->(Y)$ makes reference to the exchange between the microgrid (X) and the microgrid (Y), being $i^{exch}_{(X)->(Y)}$ the exchanged current between the microgrid (X) and the microgrid (Y). Notice that this term achieves to syncronize in frequency both microgrids and also to equilibrate the voltage magnitude between both microgrids without being necessary any kind of communication between the interconnected microgrids.

3. Simulation Results

The simulations are carried out using Simpower© using $T = 1\mu s$ as sample period while the controller acts each $T = 20\mu s$. The different values for the simulation and power inverter components are exposed in Table 1.

Table 1. Components value

Parameter	Value
Filter inductance L_f	1 mH
Filter inductance resistance R_{L_f}	0.1[Ω]
Filter capacitor C_f	0.5 [mF]
Filter capacitor resistance R_{C_f}	0.1[Ω]
DC link voltage U_{dc}	950 [V]
Neutral inductance L_N	2.5[μF]
Neutral inductance resistance R_{L_N}	0.1[Ω]
Neutral balancing capacitors C_+, C_-	6600 [μF]
Grid connection line inductance L_{grid}	0.1[mH]
Grid connection line resistance R_{grid}	0.1[Ω]
Slave inverter line inductance L_{inv}	0.1[mH]
Slave inverter line resistance R_{inv}	0.1[Ω]
Non-linear load line inductance L_{non}	0.1[mH]
Non-linear load line resistance $R_{L_{non}}$	0.1[Ω]
Non-linear load dc resistance R_{non}	60[Ω]
Non-linear load dc capacitor C_{non}	6.6 [mF]
Unbalanced load phase a resistance R_a	1 [$M\Omega$]
Unbalanced load phase b resistance R_b	10 [Ω]
Unbalanced load phase c resistance R_c	10 [Ω]
Unbalanced load phase b inductance L_b	1 [mH]
Unbalanced load phase c capacitor C_c	0.1 [mF]

3.1. Comparison between MPC and PI-PWM controllers for single microgrids

The first simulation is used in order to compare the results in both grid-connected and islanded mode, as well as the transition between modes using an MPC-controller and a PI-PWM-controller for a single microgrid working in both modes: grid-connected and islanded. In this simulation the non-linear and the unbalanced loads are connected to the microgrid in all the sample instants. Both controllers receive the next references for the power exchange with the main grid: $[P^{ref}_{grid,\alpha}, Q^{ref}_{grid,\alpha}] = [-15000\text{ W}, -9000\text{ Var}]\ \forall t \in [0\text{ s}, 0.5\text{ s}]$ and $[P^{ref}_{grid,\alpha}, Q^{ref}_{grid,\alpha}] = [+15000\text{ W}, +9000\text{ Var}]$ at $\forall t \geq 0.5$ s. Between $t \in [1s, 1.5s]$ a fault in the main grid occurs so the transition to islanded mode is required, restoring the connection of the microgrid with the main grid for $t > 1.5s$. The comparison between the results obtained in the reference tracking for the active and reactive power between the MPC and the PI-PWM controller can be found in Fig. 3. As can been seen in the figure, the PI-PWM controller presents a longer transient response while the MPC controller reaches the given references in just two cycles of the fundamental frequency. In Fig. 4, the comparison between the THD results for the MPC and PI-PWM controller are exposed. As can be seen, despite the presence of non-linear and unbalanced loads the current waveforms present a low content of harmonics in the MPC-controller while the PI-PWM controller is not able to minimize the harmonic content in the current waveform.

Preprints (www.preprints.org) | NOT PEER-REVIEWED | Posted: 4 January 2021 doi:10.20944/preprints202101.0003.v1

During the instants $t = 1$ s and $t = 1.5$ s, it occurs a grid blackout and the power inverter works in islanded mode. The comparison between the behavior of the power inverter with the MPC and the PI-PWM controllers can be seen in Fig. 5 and Fig. 6 where the voltage magnitude and the phase values are shown. As it occurs for the case of grid-connected mode, a better transient response is obtained in the case of the MPC controller. A better response is also obtained for THD values of the voltage at the Point of Common Coupling (PCC) in the case of the MPC controller as can be seen in Fig. 7.

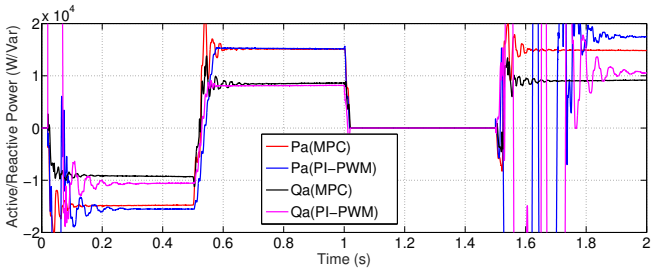

Figure 3. Comparison of the results for the active and reactive power exchange with the main grid between the MPC and PI-PWM controllers for phase *a*

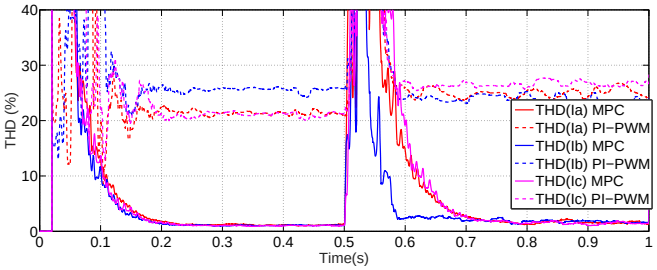

Figure 4. Comparison of the THD values for the current exchange with the main grid between the MPC and PI-PWM Controllers

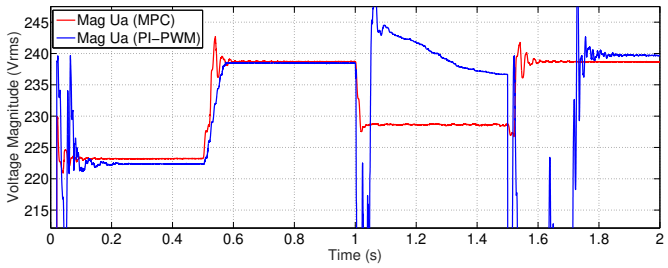

Figure 5. Voltage Magnitude for phase A at the PCC

3.2. *Power Quality Management Results for interconnected microgrids working without presence of grid*

The aim of the second simulation launched is to evaluate the behavior of the presented controller for the case of interconnected microgrids working under a grid blackout. In this case, the IPS-A and IPS-B are connected and IPS-grid is disconnected (see Fig. 1). In the case of the microgrid (A) the non-linear loads are connected during all the sample instants of the simulation and the unbalanced loads are connected for these sample instants $t > 0.2\ s$. In the microgrid (B) the unbalanced loads are connected during all the sample instants and the non-linear loads are connected at $t > 0.1\ s$. In Fig. 8 and Fig. 9 a comparison between the obtained results for the voltage magnitudes for every phase of

Preprints (www.preprints.org) | NOT PEER-REVIEWED | Posted: 4 January 2021 doi:10.20944/preprints202101.0003.v1

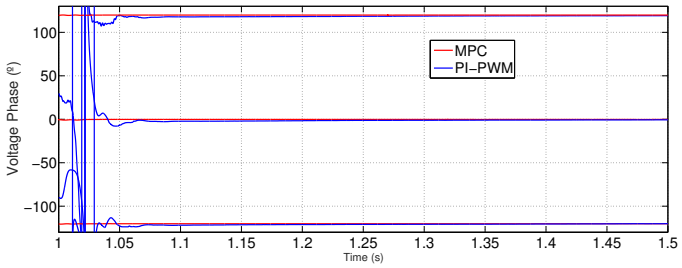

Figure 6. Absolute voltage phase angle value of the voltages at the PCC during the blackout of the main grid

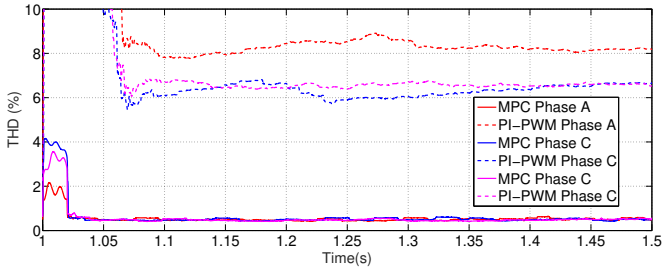

Figure 7. THD values for the voltages at the PCC during the blackout of the main grid

each microgrid are shown. The current consumption can be observed in Fig.12. As can be seen, for the sample instants $t \in [0.10, 0.12]$ in Fig. 9 a more robust behavior is obtained in the case of working interconnected where the voltage magnitudes of each microgrids are always $|\mathscr{U}_{out,\gamma}^{(X)}| > 200$ for both microgrids. In Fig.13 the obtained results for the current exchange between both microgrids are shown. As can be seen, each microgrid manages its own loads without nearly non-affection to the neighbor microgrid. As can be seen in Fig. 10 and Fig. 11, the presence of non-linear and unbalanced loads and the changes in current demand at each microgrid, as well as the interaction between microgrids do not affect to the THD content in voltage or to the balance between phases guaranteeing the power quality supply to the loads connected to both microgrids.

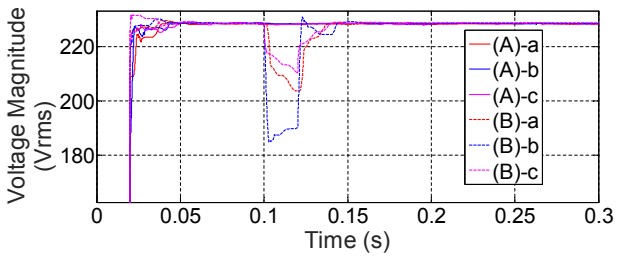

Figure 8. Voltage Magnitude per phase and microgrid in mode non-interconnected and grid-islanded

4. Conclusions

In the present study, the behavior of a new algorithm applied to control a four-wire three-phase VSI with active control of the neutral point which governs a microgrid in both modes grid-connected and islanded has been exposed. It has been developed using the finite-state MPC control technique with a control horizon equal than "1". The results show an optimal behaviour for the output variables of the inverter, with a low THD in voltage in the case of islanded and in the current exchanged with the grid in case it works as a grid-tied inverter. The difference with previous works is the use of the

Preprints (www.preprints.org) | NOT PEER-REVIEWED | Posted: 4 January 2021 doi:10.20944/preprints202101.0003.v1

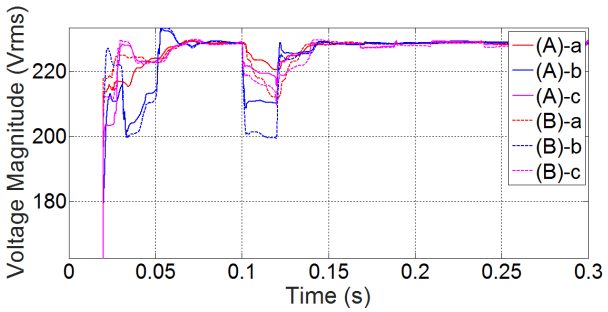

Figure 9. Voltage Magnitude per phase and microgrid in mode interconnected and grid-islanded

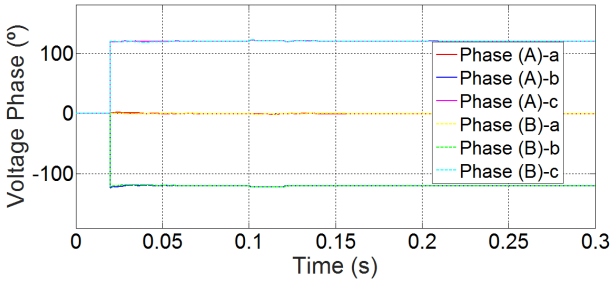

Figure 10. Absolute voltage phase angle value per phase and microgrid in mode interconnected and grid-islanded

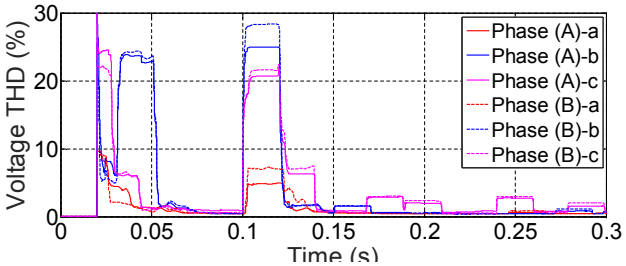

Figure 11. Voltage THD per phase and microgrid in mode interconnected and grid-islanded

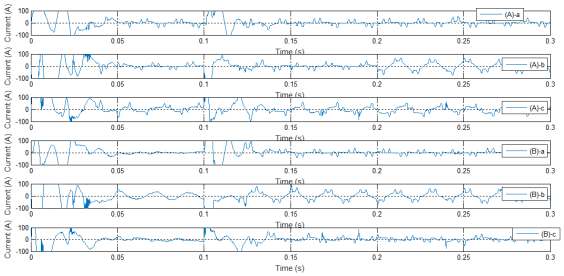

Figure 12. Current per phase and microgrid in mode interconnected and grid-islanded

mean voltage/power values evaluated in the fundamental component. This allows controlling even with the harmonic presence correcting the low horizon prediction limitation that MPC applied to power electronic has. With this method although the inverter need to be modeled the load is modeled on-line by the controller with accurate results for the current prediction in all the exposed cases with the developed technique. The inverter has been designed to act as a master of a microgrid. The most critical cases as non-linear sources, non-linear loads and umbalanced loads have been tested showing an accurate response for each one of the exposed cases. A fast transition behaviour when it is

Preprints (www.preprints.org) | NOT PEER-REVIEWED | Posted: 4 January 2021 doi:10.20944/preprints202101.0003.v1

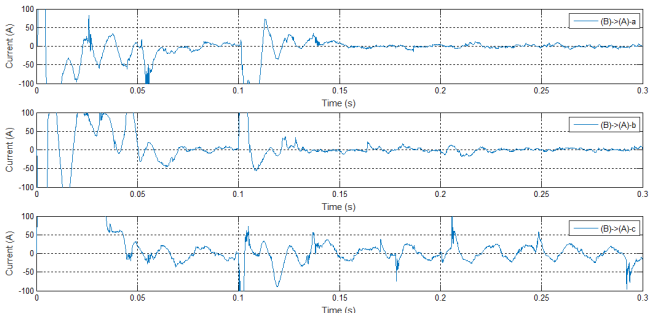

Figure 13. Current exchange per phase between microgrid (A) and microgrid (B)

required to switch the working mode is also found. The results shown that beside the non-linearities and unbalances found in the microgrid the inverter achieves with the established in the standard EN-50160 for the islanded mode in which refers to voltage harmonics content. Despite the presence of unbalanced and non-linear loads it also fulfills what corresponds with the standard IEC 61000-3-2 and IEC 61000-3-4 regarding the harmonic current emission limits for balanced system.

The controller has been also validated for the implementation to manage the power quality in interconnected microgrids acting when they are grid-connected or under a grid blackout where they have to work interconnected but islanded from the main grid. The control algorithm is based on an MPC-controller applied to a four-wire three-phase VSI with active control of the neutral point which works as master of a microgrid with unbalanced and non-linear loads and generators connected. The simulation results show the potential of the presented MPC-controller in comparison wiht classical PI-PWM controllers solving the transient response problems of traditional methods. The fact of possessing an accurate transient response is specially advantageous for power quality problems in microgrids overall if unbalanced and non-linear loads and generators are connected to the microgrids. As can be seen, the developed methodology is improved with its application to the case of interconnected microgrids acting islanded from the main grid.

Author Contributions: Conceptualization, All; methodology, All; software, FG and SV; validation, FG and SV; formal analysis, All; investigation, All; resources, All; data curation, All; writing–original draft preparation, All; writing–review and editing, All; visualization, All; supervision, All; project administration, All; funding acquisition, All

Funding: This research has been funded by European Commission with the European Regional Development Funds (ERDF) under the program Interreg SUDOESOE3/P3/E0901 (Project IMPROVEMENT)

Acknowledgments: Authors acknowledge the support given by their affiliation entities: National Center of Hydrogen (CNH2), University of Seville, University of Cordoba and University of Castilla La Mancha, in Spain for the support to carry out this study.

Conflicts of Interest: The authors declare no conflict of interest. The funders had no role in the design of the study; in the collection, analyses, or interpretation of data; in the writing of the manuscript, or in the decision to publish the results.

Abbreviations

The following abbreviations are used in this manuscript:

CCS	Continuous Control Set
DER	Distributed Energy Resources
DMPC	Distributed Model Predictive Control
ESS	Energy Storage System
FCS	Finite Control State
GPC	Generalized Predictive Control
MPC	Model Predictive Control
PQR	Power Quality and Realibility
RES	Renewable Energy System
SHE	Selective Harmonic Elimination
SP	Smith Predictor
VSI	Voltage Source Inverter

1. Bollen, M.; Zhong, J.; Zavoda, F.; Meyer, J.; McEachern, A.; Lopez, F.C. Power quality aspects of smart grids. International Conference on Renewable Energies and Power Quality (ICREPQ'10), 2010.
2. Vasquez, J.C.; Guerrero, J.M.; Miret, J.; Castilla, M.; De Vicuna, L.G. Hierarchical control of intelligent microgrids. *IEEE Industrial Electronics Magazine* **2010**, *4*, 23–29.
3. Olivares, D.E.; Mehrizi-Sani, A.; Etemadi, A.H.; Cañizares, C.A.; Iravani, R.; Kazerani, M.; Hajimiragha, A.H.; Gomis-Bellmunt, O.; Saeedifard, M.; Palma-Behnke, R.; others. Trends in microgrid control. *IEEE Transactions on smart grid* **2014**, *5*, 1905–1919.
4. Han, Y.; Li, H.; Shen, P.; Coelho, E.A.A.; Guerrero, J.M. Review of active and reactive power sharing strategies in hierarchical controlled microgrids. *IEEE Transactions on Power Electronics* **2016**, *32*, 2427–2451.
5. Rajesh, K.; Dash, S.; Rajagopal, R.; Sridhar, R. A review on control of ac microgrid. *Renewable and sustainable energy reviews* **2017**, *71*, 814–819.
6. Yu, X.; Khambadkone, A.M.; Wang, H.; Terence, S.T.S. Control of parallel-connected power converters for low-voltage microgrid—Part I: A hybrid control architecture. *IEEE Transactions on Power Electronics* **2010**, *25*, 2962–2970.
7. Vandoorn, T.L.; De Kooning, J.D.; Meersman, B.; Guerrero, J.M.; Vandevelde, L. Automatic power-sharing modification of P/V droop controllers in low-voltage resistive microgrids. *IEEE Transactions on Power Delivery* **2012**, *27*, 2318–2325.
8. Guerrero, J.M.; De Vicuña, L.G.; Matas, J.; Castilla, M.; Miret, J. Output impedance design of parallel-connected UPS inverters with wireless load-sharing control. *IEEE Transactions on industrial electronics* **2005**, *52*, 1126–1135.
9. Micallef, A.; Apap, M.; Spiteri-Staines, C.; Guerrero, J.M.; Vasquez, J.C. Reactive power sharing and voltage harmonic distortion compensation of droop controlled single phase islanded microgrids. *IEEE Transactions on Smart Grid* **2014**, *5*, 1149–1158.
10. Savaghebi, M.; Jalilian, A.; Vasquez, J.C.; Guerrero, J.M. Secondary control for voltage quality enhancement in microgrids. *IEEE Transactions on Smart Grid* **2012**, *3*, 1893–1902.
11. Bordons, C.; Garcia-Torres, F.; Ridao, M.A. *Model Predictive Control of Microgrids*; Springer, 2020.
12. Rodriguez, J.; Pontt, J.; Silva, C.A.; Correa, P.; Lezana, P.; Cortés, P.; Ammann, U. Predictive current control of a voltage source inverter. *IEEE transactions on industrial electronics* **2007**, *54*, 495–503.
13. Vazquez, S.; Montero, C.; Bordons, C.; Franquelo, L.G. Design and experimental validation of a model predictive control strategy for a VSI with long prediction horizon. IECON 2013-39th Annual Conference of the IEEE Industrial Electronics Society. IEEE, 2013, pp. 5788–5793.
14. Acuna, P.; Moran, L.; Rivera, M.; Dixon, J.; Rodriguez, J. Improved active power filter performance for renewable power generation systems. *IEEE transactions on power electronics* **2013**, *29*, 687–694.
15. Antoniewicz, K.; Jasinski, M.; Kazmierkowski, M.P.; Malinowski, M. Model predictive control for three-level four-leg flying capacitor converter operating as shunt active power filter. *IEEE transactions on industrial electronics* **2016**, *63*, 5255–5262.
16. Liu, X.; Wang, D.; Peng, Z. Cascade-free fuzzy finite-control-set model predictive control for nested neutral point-clamped converters with low switching frequency. *IEEE Transactions on Control Systems Technology* **2018**, *27*, 2237–2244.

17. Mohapatra, S.R.; Agarwal, V. Model Predictive Control for Flexible Reduction of Active Power Oscillation in Grid-tied Multilevel Inverters under Unbalanced and Distorted Microgrid Conditions. *IEEE Transactions on Industry Applications* **2019**, *56*, 1107–1115.
18. Wu, M.; Tian, H.; Li, Y.W.; Konstantinou, G.; Yang, K. A composite selective harmonic elimination model predictive control for seven-level hybrid-clamped inverters with optimal switching patterns. *IEEE Transactions on Power Electronics* **2020**, *36*, 274–284.
19. Aguilera, R.P.; Acuna, P.; Lezana, P.; Konstantinou, G.; Wu, B.; Bernet, S.; Agelidis, V.G. Selective harmonic elimination model predictive control for multilevel power converters. *IEEE Transactions on Power Electronics* **2016**, *32*, 2416–2426.
20. Shan, Y.; Hu, J.; Li, Z.; Guerrero, J.M. A model predictive control for renewable energy based ac microgrids without any pid regulators. *IEEE Transactions on Power Electronics* **2018**, *33*, 9122–9126.
21. Ahumada, C.; Cárdenas, R.; Saez, D.; Guerrero, J.M. Secondary control strategies for frequency restoration in islanded microgrids with consideration of communication delays. *IEEE Transactions on Smart Grid* **2015**, *7*, 1430–1441.
22. Garcia-Torres, F.; Valverde, L.; Bordons, C. Optimal load sharing of hydrogen-based microgrids with hybrid storage using model-predictive control. *IEEE Transactions on Industrial Electronics* **2016**, *63*, 4919–4928.
23. Kayalvizhi, S.; Kumar, D.V. Load frequency control of an isolated micro grid using fuzzy adaptive model predictive control. *IEEE Access* **2017**, *5*, 16241–16251.
24. Lou, G.; Gu, W.; Xu, Y.; Cheng, M.; Liu, W. Distributed MPC-based secondary voltage control scheme for autonomous droop-controlled microgrids. *IEEE transactions on sustainable energy* **2016**, *8*, 792–804.
25. Kerdphol, T.; Rahman, F.S.; Mitani, Y.; Hongesombut, K.; Küfeoğlu, S. Virtual inertia control-based model predictive control for microgrid frequency stabilization considering high renewable energy integration. *Sustainability* **2017**, *9*, 773.
26. Gómez, J.S.; Sáez, D.; Simpson-Porco, J.W.; Cárdenas, R. Distributed predictive control for frequency and voltage regulation in microgrids. *IEEE Transactions on Smart Grid* **2019**, *11*, 1319–1329.
27. Garcia-Torres, F.; Bordons, C.; Vazquez, S. Voltage predictive control for microgrids in islanded mode based on fourier transform. 2015 IEEE International Conference on Industrial Technology (ICIT). IEEE, 2015, pp. 2358–2363.